

Photoelectron spectroscopic study of CdS nanocrystallites

J. Nanda, Beena Annie Kuruvilla, and D. D. Sarma*

Solid State and Structural Chemistry Unit, Indian Institute of Science, Bangalore-560012, India

(Received 5 October 1998)

Nanocrystallites of semiconductors, especially those belonging to II-VI and III-V groups, show size-dependent optical and electrical properties. In this paper we report on x-ray photoemission results of CdS nanocrystallites of two different sizes and compare these results with bulk CdS. The S $2p$ and $2s$ core levels of the nanocrystallites reveal three different types of sulfur, unlike bulk CdS, which shows only one kind of sulfur species. Details of the spectroscopic results provide estimates of the size of the nanocrystallites, while also indicating the origin of the stability of such small clusters. [S0163-1829(99)03811-4]

I. INTRODUCTION

Semiconductor nanocrystallites have continued to be an active field of research for more than a decade primarily for two reasons. First, it gives a unique opportunity to study the material properties at the nanometer level and consequently to understand the underlying physics at reduced dimensions. The second reason is based on their immense potential for application in the area of optoelectronic devices. At such length scales, intermediate between two well-studied and extensively developed limits, namely, those of the atomic and molecular sizes on one hand and the macroscopic world of extended solids on the other, nanomaterials are expected to exhibit unique properties, possibly requiring new theoretical frameworks to describe their properties. The optical and electrical properties of nanocrystallites are significantly different from the corresponding bulk and depend on the crystallite size.¹⁻⁴ Blueshift of the optical absorption and fluorescence band with decrease in the crystallite size, higher oscillator strengths, and enhanced nonlinear optical coefficients are some examples of the interesting properties exhibited by semiconductor nanocrystallites. These size-dependent properties arise from quantum confinement as a direct consequence of the reduction in the crystallite size.⁵⁻⁷ Briefly, when the size of the crystallites are on the order of a few nanometer or even less, the photogenerated carriers, i.e., electrons and holes, feel the spatial confinement; as a consequence of this the electronic energy levels shift to the higher energy. This leads to an increase in the band gap. In molecular terminology, this is referred to as an increase in the HOMO-LUMO gap. However, the extent of the increase in the band gap with size depends on the specific type of the semiconductor sample and the effective mass of carriers. For example, CdS shows a strong confinement effect when the size of the crystallites is around 50 Å and below, whereas PbS shows such effects even at 180 Å.⁴ Improved synthetic and fabrication methods over the last few years have paved the way to tailoring the properties of these semiconductor nanocrystallites for desired applications and also to study their properties in well-defined and properly characterized samples.

CdS is a typical II-VI semiconductor having a band gap of 2.4 eV at room temperature. Bulk CdS is widely used as a commercial photodetector in the visible spectrum; it also

finds application as a window material in heterojunction thin-film solar cells.⁸ The photophysical and optical properties of CdS nanocrystallites have been extensively studied^{9,10} as this system is known to exhibit pronounced quantum size effect. These nanocrystallites display a wide range of interesting properties. Apart from their unique absorption and luminescence properties, which makes them suitable materials for application as optoelectronic devices, they also exhibit exciting thermodynamical and structural properties. Lowering of the melting point with reduced size of the crystallites and pressure-induced structural transformations¹ are just two examples of such exotic properties. Optical and structural studies of CdS nanocrystallites have already been extensively studied, but there has been very little work to date on the photoemission aspects of these nanocrystallites.¹¹ While optical spectroscopy of the nanocrystallites provides information about the band to band transitions and their relative positions thus giving an estimate of the band gap (for direct band-gap semiconductors), photoemission experiments, on the other hand, probe the detail structure of the valence band and the absolute energy position of the band edges.¹¹ Moreover, photoemission core levels give a quantitative idea of the chemical shift and other bonding aspects including the nature of the surface passivation, which plays an important role in controlling the optical and electrooptical properties. There are hardly any studies on these aspects, particularly with reference to II-VI nanocrystalline semiconductors, like CdS. In fact, the powerful techniques of electron spectroscopy have in general been underutilized in the study of semiconducting nanocrystals, in spite of the proven efficacy of these spectroscopic methods to effectively probe a wide variety of physical and chemical phenomena. In this article we discuss x-ray photoemission (XP) spectra of CdS nanocrystallites with two different sizes in the quantum confinement limit, compared to the bulk CdS. We discuss in detail the various features of the Cd $3d$ and S $2p$ core levels, which provide an understanding of the composition and the stability of these nanocrystals. Furthermore, we show for the first time that it is possible to estimate the size of the nanocrystallites from such core-level spectral analysis measurements.

II. EXPERIMENTAL DETAILS

CdS nanocrystallites having an average diameter of 25 Å and 45 Å, hereafter called CdS-I and CdS-II, respectively,

were synthesized following the procedure reported earlier.¹² The synthesis method, in brief, consists of refluxing the reaction mixture containing fixed amount of cadmium acetate and thiourea in the presence of a capping agent 1-thioglycerol in an organic solvent dimethyl formamide (DMF). In the case of the smaller (25 Å) cluster, the refluxed solution was subjected to a method known as size selective precipitation¹³ in order to separate out the larger CdS particles giving a narrow size distribution. In this procedure, one finally obtains free standing powders of CdS nanocrystallites that remain stable for several months. The optical absorption spectra of the nanocrystallites in the ultraviolet-visible (UV-vis) range were recorded using a Hitachi UV-vis spectrophotometer using a thin-film sample of these nanocrystallites on a quartz plate. The thin film of the nanocrystallites was prepared by spin coating the quartz plate with a solution of the nanocrystallites in DMF. X-ray diffraction patterns of the nanocrystallites were recorded in the step scan mode with a Siemens D5005 diffractometer using Cu K_{α} radiation having a net x-ray power of 900 W. Since the diffracted intensities from such nanocrystallite systems are generally weak, all patterns were recorded at a slow scan rate (10 sec per 0.1°) in order to get a reasonable signal to noise ratio.

The x-ray photoelectron spectra were recorded with a commercial electron spectrometer from VSW Scientific Instruments using a monochromatized Al K_{α} source. The total resolution of the spectra reported here is approximately 0.5 eV. All of the spectra were recorded at a base pressure of 5×10^{-10} mbar. The samples exhibited finite charging up leading to a shift of the measured binding energies, on account of their insulating nature. We adopted the following procedure to eliminate such charging effects. The nanocrystallite powders were thoroughly mixed with powdered graphitic carbon. This allows the nanocrystallites to be finely dispersed and be in intimate contact with conducting graphite surfaces without agglomerating into macroscopic lumps that are insulating. The graphite layer on the nanocrystal surface serves as a conducting path for the charges that tend to accumulate due to the photoemission process. We ensured that there was no charging in the samples by recording the intense and narrow Cd $3d$ peak with varying x-ray power. There was no noticeable shift in the Cd $3d$ binding energy with x-ray power ranging between 40 and 120 W.

III. RESULTS AND DISCUSSION

The UV-vis absorption spectra of the nanocrystallite films of both sizes are shown in Fig. 1. These spectra of the nanocrystallites are distinctly different compared to the well-known featureless absorption edge of bulk CdS that appears at approximately 515 nm.¹⁴ We have marked the absorption edge position of bulk CdS with an arrow in Fig. 1. In contrast, the spectra from nanocrystallites are structured with the absorption edge of the CdS-I being approximately 400 nm and that of the CdS-II at 450 nm. The structures in the absorption spectrum of CdS-I and CdS-II correspond to the excitonic transitions in the nanocrystallites. The peaks at 375 nm for CdS-I and at 410 nm for CdS-II have been attributed to $1S_e-1S_h$ transition.¹² In CdS-I we notice another peak at approximately 305 nm that corresponds to a higher-order excitonic transition. Such sharp absorption spectra with clear

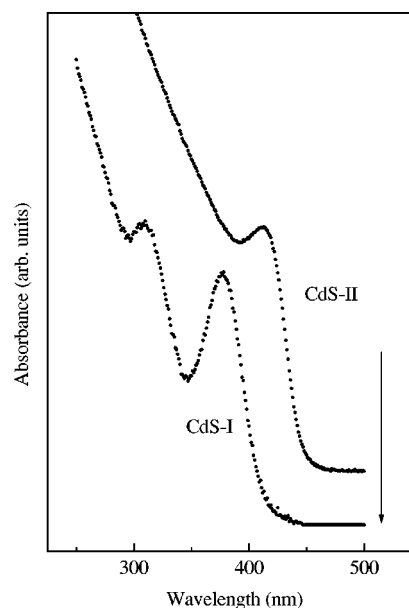


FIG. 1. UV-vis optical absorption of CdS-I and CdS-II nanocrystallites. The absorption edge of bulk CdS is shown by an arrow.

excitonic features indicate a narrow size distribution of the nanocrystallites; otherwise a large size distribution would have resulted in a wide distribution of the band gaps yielding a broad and featureless optical absorption edge. It is clear from the experimental spectra that there is a large shift of the absorption edges of the nanocrystallites towards lower wavelength (higher energy), systematically increasing with decreasing crystallite size. The band gaps calculated from the first excitonic peak maxima of the absorption spectra are approximately 3.35 eV and 3 eV for CdS-I and CdS-II, respectively, as compared to a band gap of 2.4 eV in bulk CdS. Lippens and Lanoo using a semiempirical tight-binding scheme have calculated the lowest excited state of the CdS nanocrystallites as a function of the crystallite size.¹⁵ These calculated results suggest band gaps of 3.1 eV and 2.75 eV for nanocrystallite sizes of 25 and 45 Å, which agree reasonably well with the experimentally obtained band gaps from the optical absorption measurements in the present study. On the other hand, calculations based on the effective mass approximation by Brus and others¹⁶ yield band gaps of approximately 3.9 eV and 2.9 eV for the 25 Å and 45 Å nanocrystallites, respectively.

The x-ray diffraction patterns of the nanocrystallites are shown in Fig. 2. We have also shown the pattern of bulk CdS corresponding to the wurtzite phase for comparison. Both CdS-I and CdS-II nanocrystallites show considerable broadening in the x-ray pattern in comparison to the diffraction pattern obtained from bulk CdS; this broadening of the diffraction peaks is primarily due to the finite size of the nanocrystallites and is quantitatively given by the Debye-Scherrer formula.¹⁷ However, it is clear from the figure that CdS-II nanocrystallites show clear signatures of the wurtzite phase of the bulk sample. It has also been reported that CdS nanocrystallites in a particular size regime exhibit a mixture of zinc-blende and wurtzite structures.¹⁸ Such a mixture of crystallographic phases also exists in the case of CdSe nanocrystallites as shown by the x-ray simulation results of Bawendi and co-workers.¹⁹ The x-ray diffraction pattern of

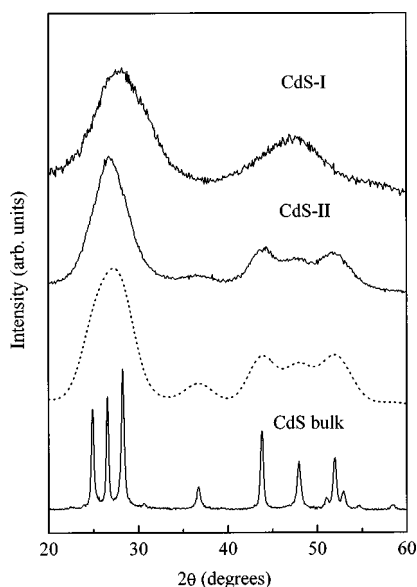


FIG. 2. X-ray diffraction pattern of CdS-I and CdS-II. The bulk CdS pattern corresponding to the wurtzite phase is also shown for comparison. The dotted lines show the calculated fit to CdS-II nanocrystallites, as described in the text.

CdS-I nanocrystallites is broadened considerably more compared to that of CdS-II due its smaller size. This pattern does not exhibit the characteristic features of the wurtzite structure, possibly due to the extensive broadening of the line shape; therefore, it is difficult to obtain any meaningful information about the structural phase purity of this sample from the x-ray pattern. It is possible that the smaller-size CdS-I particles are formed in a crystallographically mixed phase of hexagonal and cubic structures, as reported earlier for various size CdS nanocrystals.

In an attempt to obtain more quantitative analysis of the x-ray pattern corresponding to CdS-II nanocrystallites, the experimental bulk x-ray diffraction pattern was convoluted with a Gaussian the full width at half-maximum (FWHM) of which is related to the coherence length (L), and the diffraction angle (θ) by the Debye-Scherrer formula as

$$L = \frac{0.9\lambda}{B \cos \theta}.$$

In the case of spherical crystallites, the relation between the coherence length L and the crystallite size D is given by $L = \frac{4}{3}D$. λ is the wavelength of the x-ray radiation, B is the full width at half-maximum and θ is the angle of reflection of the peak. We find that the broad peak ranging from the 2θ value of 24–30° in the CdS-II pattern is actually a convolution of three peaks (shown in the case of the bulk) each being broadened by the finite-size effect; we obtain a good description for this diffraction feature, if we assume the value of L to be 25 Å, which corresponds to a diameter D of approximately 33 Å, as shown by the dotted line in Fig. 2; this value is somewhat smaller than that estimated from the band edge shift observed in the UV-vis absorption spectrum in Fig. 1. Such underestimation of the size obtained from the x-ray diffraction line broadening could possibly arise from the fact that these samples are not fully annealed, resulting in a poor crystallinity and/or the fact that there may be several crys-

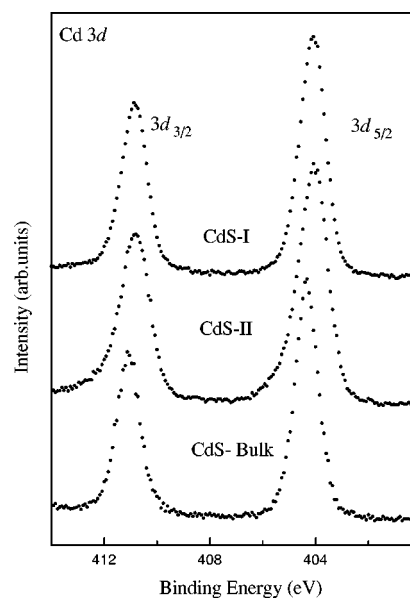


FIG. 3. X-ray photoemission spectra of Cd 3d core levels from CdS-I, CdS-II, and bulk CdS.

talline domains in a single nanocrystallite. We notice that while the fit is reasonably good for $L = 25$ Å at lower 2θ values, this is not true for the higher 2θ values in which the experimental spectrum is broader than the calculated fit. This extra broadening at higher angles is primarily due to several defects, stacking faults and distortions,¹⁹ which are intrinsic to such samples.

The Cd 3d levels of the nanocrystallites and bulk CdS are shown in Fig. 3. The 3d spectrum in each case has a doublet feature due to the spin-orbit splitting resulting into $3d_{5/2}$ and $3d_{3/2}$ peaks with a spin-orbit separation of 6.7 eV. The binding energies of $3d_{5/2}$ and $3d_{3/2}$ of bulk CdS are 404.4 eV and 411.1 eV. In the case of nanocrystallites, the Cd 3d levels are slightly broadened and also shifted towards lower binding energy by about 0.3 eV. Such small shifts in the binding energies of metal core levels in nanocrystallite samples have been reported earlier²⁰ in the case of PbI_2 . We find that the Cd 3d levels of nanocrystallites show only a single peak feature in each of the spin-orbit component without any evidence for a second Cd species, in close similarity with the spectrum of bulk CdS. This indicates that all cadmium sites are essentially equivalent, in a similar chemical environment, bonded to sulfur without any extraneous impurity phases in these nanocrystallite samples. Apart from Cd 3d, other core levels of interest in these materials are S 2p and S 2s. These are shown in Fig. 4 for bulk CdS. The sulfur 2p spectrum exhibits a doublet arising from the spin-orbit split $2p_{3/2}$ and $2p_{1/2}$ spectral features at binding energies 162.3 and 163.4 eV. The experimental S 2p spectrum of bulk CdS [Fig. 4(a)] can be described with two Gaussians having the same FWHM of 0.44 eV and separated by a spin orbit splitting of 1.2 eV as shown by the solid line superimposed on the experimental spectrum; the triangles show the error in the fit at each point. The S 2s spectrum has a single peak feature appearing at a binding energy of 225 eV [Fig. 4(b)]. As expected, the S 2p and S 2s spectral features from bulk CdS are consistent with a single sulfur species being present, confirming the absence of any impurity feature. In contrast, S

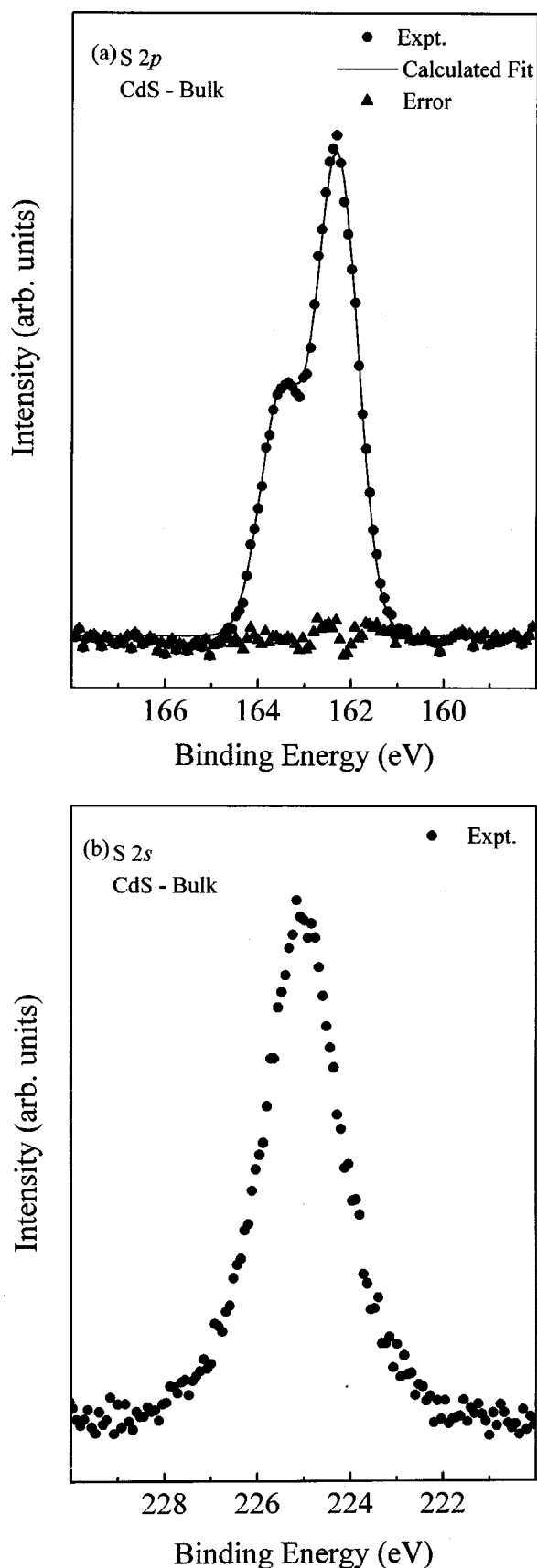


FIG. 4. X-ray photoemission spectra of bulk CdS, shown after removal of the inelastic background, for (a) S 2*p* and (b) S 2*s* core levels. The experimental spectra are shown by solid circles, the solid line in (a) is the calculated fit and the triangles show the errors in the fit at each point.

2*p* spectrum of CdS-I shows interesting multiple features [Fig. 5(a)] and consequently, the S 2*p* spectrum cannot be described in terms of a single set of two Gaussians representing the spin-orbit doublet as in the case of bulk CdS. In order to interpret the data quantitatively, we fitted the spectrum with multiple set of spin-orbit doublets. In this case a good fit to the experimental spectrum was obtained by three sets of doublet Gaussian functions (labeled 1, 2, and 3) with the 2*p*_{3/2} signal centered at 161.8, 162.9, and 163.9 eV, respectively; in every case the spin-orbit splitting of these three doublet Gaussian functions turns out to be 1.2 eV, as in the case of bulk CdS. The individual doublet Gaussian components are shown by dotted lines with the solid line showing the overall fit superimposed on the experimental data in Fig. 5(a). In order to ensure that the spectral decomposition shown in Fig. 5(a) for the S 2*p* spectrum is meaningful, we carried out the following consistency check. The S 2*s* spectrum from the same sample was also described in terms of three single Gaussians with energy separations and the intensity ratios being fixed to those obtained from the analysis of the S 2*p* spectrum. The fitted spectrum of S 2*s* with the above-mentioned constraints was found to provide a very good description of the experimental spectrum as shown in Fig. 5(b). In order to understand the nature of these three sulfur species, we also recorded the sulfur 2*p* and 2*s* core levels using Mg *K*_α source (not shown here). Since the photon energy of the Mg *K*_α radiation is smaller than that of Al *K*_α, photoelectron spectrum obtained with Mg *K*_α is more sensitive to the surface region. We find that these spectra are also composed of three distinct signals. Spectral decomposition as in the case of Al *K*_α showed an enhancement of the spectral features labeled 2 and 3 compared to 1, with the maximum enhancement for the feature 3. This helps us to attribute the sulfur species with the maximum intensity and the lowest binding energy (labeled 1) to the sulfur atoms of the CdS nanocluster core, the feature at the next higher binding energy (labeled 2) to the surface sulfur atoms of the CdS nanocrystallites, and the third one to the sulfur in the capping material thiolglycerol.

We show the S 2*p* and 2*s* core level spectra of CdS-II nanocrystals with an average size of 45 Å in Figs. 6(a) and 6(b), respectively. Both of these spectra are considerably narrower than the corresponding ones from the smaller-size CdS-I nanocrystal, shown in Fig. 5. However, these spectra also exhibit evidence of multiple components compared to the spectra from bulk CdS shown in Fig. 4. We have analyzed the spectra in Figs. 6(a) and 6(b) in terms of the signal arising from three distinct species of sulfur in a way exactly like that employed for CdS-I nanoparticles; we find that the spectra are well described once again in terms of three components, as shown by the fit (solid lines) and the three components (dashed lines) in Fig. 6. The energy separation between the three features as well as their widths are very similar to those obtained in the case of CdS-I nanoparticles (see Fig. 5). The main difference in this case is an evident increase of the relative intensity of the component labeled 1. Since this sulfur species is associated with the photoemission from the core of the nanocrystals, the pronounced increase in the intensity of this feature is consistent with the larger particle size of CdS-II, enhancing the ratio of bulk to surface sulfur species. Table I shows the values of the intensities of

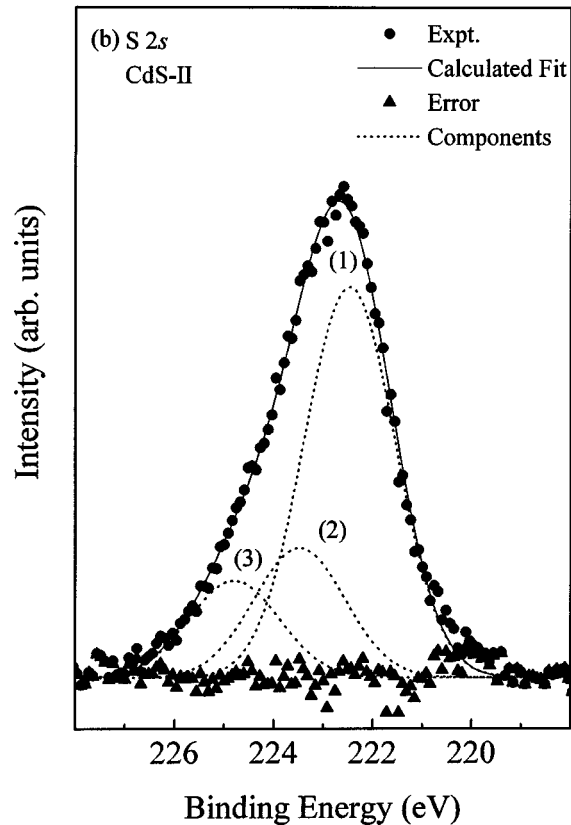
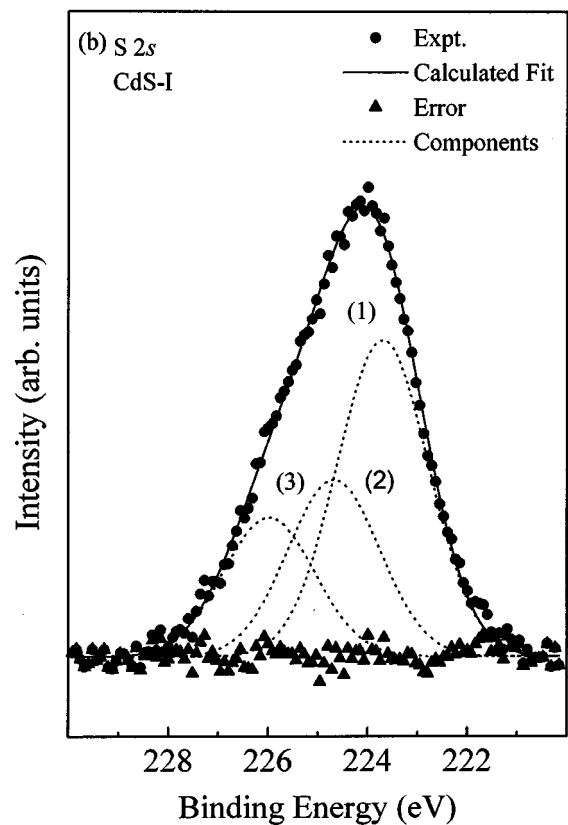
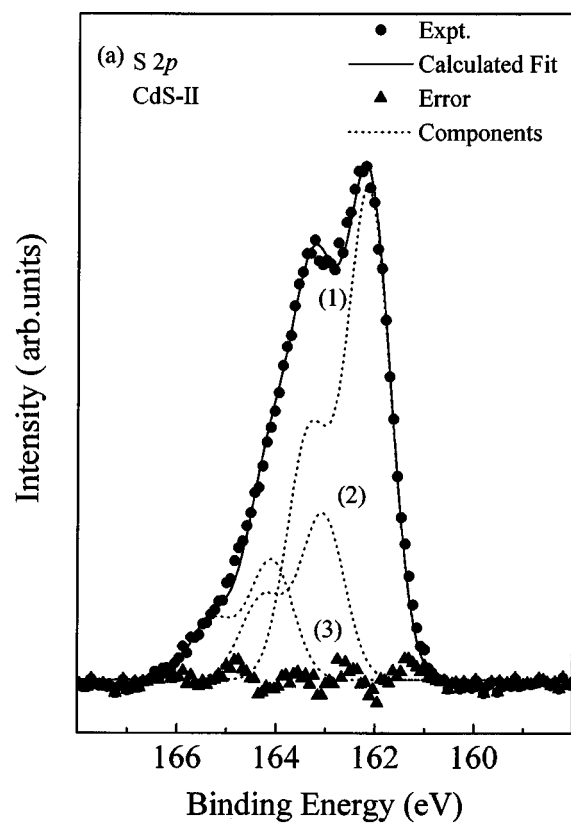
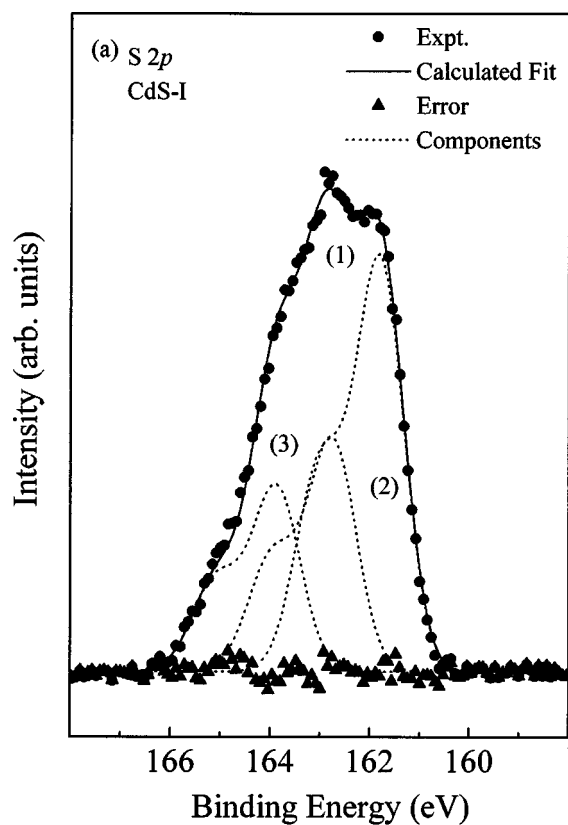


FIG. 5. X-ray photoelectron spectra of CdS-I, shown after removal of the inelastic background, for (a) S 2p and (b) S 2s core levels. The experimental spectra are shown by solid circles. The dashed lines are the individual sulfur components labeled 1, 2, and 3, respectively, the solid lines show the overall fit, and the triangles show the errors in the fit at each point.

FIG. 6. X-ray photoelectron spectra of CdS-II, shown after removal of the inelastic background, for (a) S 2p and (b) S 2s core levels. The experimental spectra are shown by solid circles. The dashed lines are the individual sulfur components labeled 1, 2, and 3, respectively, the solid lines show the overall fit, and the triangles show the errors in the fit at each point.

TABLE I. Experimentally obtained intensities of the three sulfur species, namely, the core (1), surface (2), and capping (3), in percentage of the total intensity.

Type	I_{core}	I_{sur}	I_{cap}
CdS-I	49.8	28	22.2
CdS-II	63.3	21	15.7

different sulfur components obtained by calculating the area under the curve of each type of sulfur in both the nanocrystals (I and II). The intensities corresponding to the core, surface and the capping sulfurs are referred to as I_{core} , I_{sur} , and I_{cap} , respectively. The spectral features discussed so far indicate qualitatively the structure of these nanocrystals with a core region, a surface region, and a capping layer as illustrated schematically in Fig. 7. Within the core region, the system is essentially a single-phasic CdS, as evidenced by the clean Cd $3d$ signal from the CdS nanocrystals, similar to that obtained from the bulk CdS (see Fig. 3). This core region appears to be crystalline, at least for the larger-size CdS-II nanocrystals, as suggested by the x-ray diffraction pattern, the widths of the diffraction pattern being consistent with the particle size [Fig. 2]. The surface of the CdS nanocrystallite core appears to be preferentially terminated by the sulfur ions which give rise to characteristically shifted sulfur $2p$ and $2s$ core-level peaks (labeled 2 in Figs. 5 and 6). The entire CdS nanocrystallite is stabilized by attaching thioglycerol on the surface of the clusters with the sulfurs in this capping agent exhibiting another chemically distinct species with separated core-level spectral features (labeled 3 in Figs. 5 and 6). We now turn to a more quantitative analysis of the spectral intensities summarized in Table I.

Based on these spectral decompositions of S $2p$ and S $2s$ core levels, we can model a single nanoparticle as a core-shell structure having an inner CdS core, surface CdS layer, and finally the capping layer as shown schematically in Fig. 7. An electron being photoionized below the surface of the nanocluster has a finite probability of escaping through the surface without suffering any inelastic processes and therefore being detected as a photoelectron. This probability is conveniently expressed in terms of the mean free path λ of the photoionized electron and is proportional to

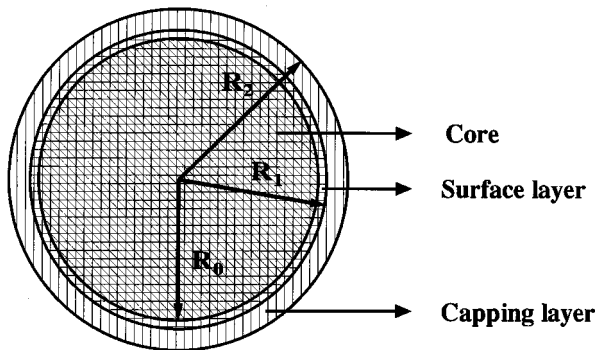


FIG. 7. Schematic model of a CdS nanocrystallite based on the photoemission core-level analysis. R_0 is the radius of the core, R_1 is the radius of the surface layer, and R_2 is the radius of the capping layer.

$\exp(-z/\lambda)$, where z is the distance between the surface and the point of origin of the photoelectron. Thus, the infinitesimal intensity contribution dI from a volume element dv is given by

$$dI = I_o \exp\left(-\frac{z}{\lambda}\right) dv, \quad (1)$$

where the normalization constant I_o depends on the particular electronic level involved and the specific sample via the photoionization cross section, as well as various instrumental factors, such as the geometry and the angular acceptance of the analyzer, the transmission coefficient, and the photon flux. Thus, integrating the above expression for the infinitesimal intensity contribution over suitable limits, one can easily obtain the total intensity from each of the three regions of the nanocrystals. It is reasonable to assume that the normalization constant, I_o has the same value (I_o^{CdS}) for S $2p$ electrons from CdS bulk and surface; however, I_o for the capping layer I_o^{Thio} is expected to be different. The experimental setup defines all the parameters related to the geometrical aspects as well as the analyzer parameters in an identical way between the various layers of nanocrystals. Thus, the difference between I_o^{Thio} and I_o^{CdS} arises from the fact that the number densities of sulfur ions in thioglycerol and CdS are different. This is easily evaluated from the physical parameters of these two compounds and can be expressed as

$$\frac{I_o^{Thio}}{I_o^{CdS}} = \frac{\rho^{Thio}}{M^{Thio}} \times \frac{M^{CdS}}{\rho^{CdS}} = 0.35,$$

where ρ^{Thio} and ρ^{CdS} are the densities and M^{Thio} and M^{CdS} are the molecular weights of the capping agent, thioglycerol, and CdS, respectively. We also need to know the value of the mean free path, λ . It is known²¹ that the electrons with sufficient kinetic energies have λ given by $\lambda = 0.5(KE)^{1/2}$ Å; this yields an estimate of λ to be approximately 18 Å for the S $2p$ core-level electrons excited with Al K_α photons ($KE = 1320$ eV). In order to estimate the various intensities from a nanocrystal, schematically shown in Fig. 7, it is convenient to express the total intensities I from each region in terms of the spherical polar coordinates with the center of the nanocrystal as the origin. This is given by

$$I = I_o \int_{R'}^{R''} \int_0^\pi \int_0^{2\pi} \exp\left(\frac{-f(r)}{\lambda}\right) r^2 dr \sin \theta d\theta d\phi, \quad (2)$$

where, $f(r) = (R^2 - r^2 \sin^2 \theta)^{1/2} - r \cos \theta$ and the r integration is over the suitable limits. It is obvious that the integration of ϕ is trivial because of the symmetry, giving a factor of 2π in every case. Since we have intensity ratios from different shells of the nanocrystals, this factor of 2π can be eliminated. Noting that R_0 is the radius of the core, R_1 the radius including the surface layer, and R_2 , the radius including the capping layer; the intensity ratios of the surface to the core and the capping to the core can be expressed as

TABLE II. Sizes of the various regions in the nanocrystals, CdS-I and -II, obtained from an analysis of the photoelectron intensity given in Table I. The symbols R_0 , R_1 and R_2 are defined in Fig. 7. The values of an average nanocrystal size (R^*) obtained from Ref. 12 are also shown for comparison. All values are in Å.

Type	Core radius R_0 (in Å)	Surface layer radius R_1 (in Å)	Capping layer radius R_2 (in Å)	Radius from expt. R^* (in Å)
CdS-I	10	11.5	13.5	13
CdS-II	20.5	22.0	24.5	22

$$\frac{I_{sur}}{I_{core}} = \frac{I_o^{CdS} \int_{R_0}^{R_1} \int_0^\pi \exp\left(\frac{-f(r)}{\lambda}\right) r^2 dr \sin \theta d\theta}{I_o^{CdS} \int_0^{R_0} \int_0^\pi \exp\left(\frac{-f(r)}{\lambda}\right) r^2 dr \sin \theta d\theta}, \quad (3)$$

$$\frac{I_{cap}}{I_{core}} = \frac{I_o^{Thio} \int_{R_1}^{R_2} \int_0^\pi \exp\left(\frac{-f(r)}{\lambda}\right) r^2 dr \sin \theta d\theta}{I_o^{CdS} \int_0^{R_0} \int_0^\pi \exp\left(\frac{-f(r)}{\lambda}\right) r^2 dr \sin \theta d\theta}. \quad (4)$$

The above integrals cannot be evaluated analytically, and thus were computed numerically for different choices of R_0 , R_1 , and R_2 . From this, the sizes of various regions in nanocrystals were estimated in the following way. The values of R_0 , R_1 , and R_2 were varied so that the calculated intensity ratios given in Eqs. (3) and (4) matched the ratios obtained by fitting the experimental spectrum and tabulated in Table I. In this way it was possible to obtain a consistent set of values for R_0 , R_1 , and R_2 for both CdS-I and II nanocrystals; these estimates of the various radii of the core-shell structure are given in Table II along with estimated sizes obtained from UV-vis absorption and transmission electron microscopy (TEM) for the sake of comparison. It should, however, be noted that the estimates from TEM and UV-vis absorption spectra do not take into account the thickness of the organic capping layer, and thus these estimates

should only be compared with the values of R_1 estimated here from the XPS analysis. Table II shows that the sizes estimated from XPS analysis agree well with the TEM results given in Ref. 12 and also with the size versus band gap relationship from the optical absorption spectra of both CdS-I and CdS-II nanocrystallites as discussed earlier, establishing the efficacy of estimating nanocrystal sizes by this approach of analyzing the core-level photoelectron spectra.

In conclusion, we have shown that core-level photoemission spectra yield important information about the bonding and surface electronic structure of CdS nanocrystalline systems. Since the mean escape depth of the photoelectrons are on the same order of magnitude as the size of these nanocrystals, it is possible to obtain detailed information about the size of the nanocrystals from the core-level analysis; using the chemically shifted binding energies of the S $2p$ core levels related to different sulfur species in the system, it has been possible for the first time to estimate the sizes of the various regions in the nanocrystallites. It is found that these nanocrystals are indeed stabilized by the presence of a surface capping layer which provides a distinctly separated core level photoemission signal.

ACKNOWLEDGMENTS

We thank Professor C. N. R. Rao for continued support. This project was funded by the Department of Science and Technology, Government of India.

*Also at Jawaharlal Nehru Center for Advance Scientific Research, Jakkur, Bangalore-560064, India. Electronic address: sarma@sscu.iisc.ernet.in

¹A. P. Alivisatos, *J. Phys. Chem.* **100**, 13 226 (1996).

²H. Weller, *Angew. Chem. Int. Ed. Engl.* **32**, 41 (1993).

³A. D. Yoffe, *Adv. Phys.* **42**, 173 (1993).

⁴Y. Wang and N. Herron, *J. Phys. Chem.* **95**, 525 (1991).

⁵L. Brus, *Appl. Phys. A: Solids Surf.* **53**, 465 (1991).

⁶Yosuke Kayanuma, *Phys. Rev. B* **38**, 9797 (1988).

⁷Ying Wang and Norman Herron, *Phys. Rev. B* **42**, 7253 (1990).

⁸W. I. Danaher, L. E. Lyons, and G. C. Morris, *Sol. Energy Mater.* **12**, 137 (1985).

⁹J. Nanda, K. S. Narayan, Beena Annie Kuruvilla, G.L. Murthy, and D. D. Sarma, *Appl. Phys. Lett.* **72**, 1335 (1998).

¹⁰V. L. Colvin, M. C. Schlamp, and A. P. Alivisatos, *Nature (London)* **370**, 354 (1994).

¹¹V. L. Colvin, A. P. Alivisatos, and J. G. Tobin, *Phys. Rev. Lett.* **66**, 2786 (1991).

¹²T. Vossmeier, L. Katsikas, M. Giersig, I. G. Popovic, K. Diesner, A. Chemseddine, A. Eychmuller, and H. Weller, *J. Phys. Chem.* **98**, 7665 (1994).

¹³C. B. Murray, D. J. Norris, and M. G. Bawendi, *J. Am. Chem. Soc.* **115**, 8707 (1993).

¹⁴A. Hengliem, *Chem. Rev.* **89**, 1861 (1989).

¹⁵P. E. Lippens and M. Lannoo, *Phys. Rev. B* **39**, 10 935 (1989).

¹⁶L. E. Brus, *J. Chem. Phys.* **79**, 5566 (1983); L. E. Brus, *ibid.* **80**, 4403 (1984).

¹⁷A. Guinier, *X-Ray Diffraction* (Freeman, San Francisco, in press).

¹⁸C. Ricolleau, L. Audinet, M. Gandais, and T. Gacoin (unpublished).

¹⁹M. G. Bawendi, A. R. Kortan, M. L. Steigerwald, and L. E. Brus, *J. Chem. Phys.* **91**, 7282 (1989).

²⁰A. Roy, D. D. Sarma, and A. K. Sood, *Spectrochim. Acta* **2**, 1779 (1989).

²¹*Photoemission in Solids*, edited by M. Cardona and L. Ley (Springer-Verlag, New York, 1978), Vol. 1.